NANO LETTERS

2006
Vol. 6, No. 4
827−832

Nanorice: A Hybrid Plasmonic Nanostructure

Hui Wang,[†,||] Daniel W. Brandl,[‡,||] Fei Le,[‡,||] Peter Nordlander,[‡,§,||] and Naomi J. Halas*[,†,§,||]

Department of Chemistry, Department of Physics and Astronomy, Department of Electrical and Computer Engineering, and the Laboratory for Nanophotonics, Rice University, Houston, Texas 77005

Received January 27, 2006; Revised Manuscript Received February 28, 2006

ABSTRACT

We have designed and fabricated a new hybrid nanoparticle that combines the intense local fields of nanorods with the highly tunable plasmon resonances of nanoshells. This dielectric core–metallic shell prolate spheroid nanoparticle bears a remarkable resemblance to a grain of rice, inspiring the name "nanorice". This geometry possesses far greater structural tunability than either a nanorod or a nanoshell, along with much larger local field intensity enhancements and far greater sensitivity as a surface plasmon resonance (SPR) nanosensor than any dielectric–metal nanostructures reported previously. Invoking the plasmon hybridization picture allows us to understand the plasmon resonances of this geometry, as arising from a hybridization of the primitive plasmons of a solid spheroid and an ellipsoidal cavity inside a continuous metal.

Metals have unusual optical properties and, under reduced dimensionality, can manipulate light in unique ways. The interaction of light with the free electrons in a metal gives rise to collective oscillations of the charge density at optical frequencies, known as surface plasmons.[1,2] Metallic nanostructures have attracted a dramatic increase in attention recently because of their plasmonic properties, which allows for the development of fundamentally new metal-based subwavelength optical elements with broad technological potential, an emerging field known as plasmonics.[3−7] Metallic nanostructures possess geometry-dependent localized plasmon resonances, which is one of the major reasons for the growing interest in a rapidly expanding array of metallic nanoparticle geometries, such as nanorods,[8,9] nanorings,[10] nanocubes,[11] and nanoshells.[12] The resonant excitation of plasmons also leads to large enhancements of the local electromagnetic field at the nanoparticle surface, resulting in dramatically large cross sections for nonlinear optical spectroscopies such as surface-enhanced Raman scattering (SERS).[13−17] However, how to rationally design and controllably fabricate nanostructures that combine highly structurally tunable plasmon resonances with large, well-defined local optical fields is still an open question.

Two types of metallic nanostructures that most characteristically illustrate the geometry-dependent plasmon resonant properties of this family of nanoparticles are cylindrical nanoparticles, commonly called nanorods,[8,18,19] and dielectric core−metal shell nanoparticles, known as nanoshells.[12] Nanorods possess two plasmon resonances corresponding to the oscillation of electrons along the longitudinal and transverse axes of the nanoparticle; by changing the length of the nanorod, the longitudinal plasmon resonance frequency can be tuned systematically. Nanoshells possess two tunable resonances arising from the hybridization of the plasmons on the inner surface of the shell with the plasmons on the outer shell surface and can be tuned by varying the relative size of the inner and outer radius of the metallic shell layer.[20,21] The geometrically sensitive hybrid plasmon resonances of nanoshells are rigorous mesoscopic analogues of the hybridized electronic wave functions of simple atoms and molecules. Thus, the two plasmon resonances of a nanoshell are denoted as "bonding" and "antibonding" plasmons, in direct analogy with molecular orbital theory.

Here we report a new hybrid nanoparticle geometry that combines the plasmonic properties of both nanorods and nanoshells in a single structure. This dielectric core−metallic shell prolate spheroid nanoparticle bears a remarkable resemblance to a grain of rice, inspiring the name "nanorice". Nanorice is composed of a spindle-shaped hematite core coated with a continuous nanometer-thick Au shell. To apply the plasmon hybridization picture to analyze the resonances of this layered nanoparticle geometry, we analyze the plasmon resonances of a solid metallic nanorod and a nanocavity of arbitrary ellipticity as the parent plasmons which, when hybridized, give rise to the plasmon resonances of nanorice. Within this hybrid nanoparticle geometry we

* Corresponding author. E-mail: halas@rice.edu.
[†] Department of Chemistry.
[‡] Department of Physics and Astronomy.
[§] Department of Electrical and Computer Engineering.
[||] Laboratory for Nanophotonics.

10.1021/nl060209w CCC: $33.50
Published on Web 03/11/2006

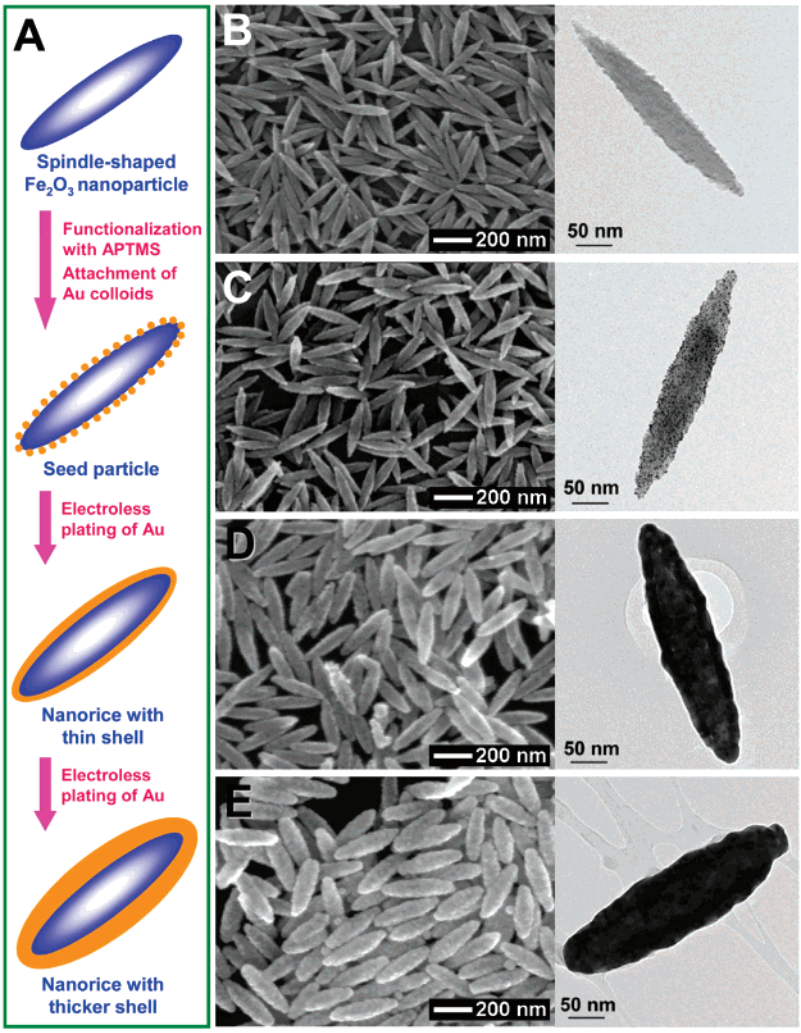

Figure 1. (A) Schematics of the fabrication of hematite−Au core−shell nanorice particles. SEM (left) and TEM (right) images of (B) hematite core (longitudinal diameter of 340 ± 20 nm, and transverse diameter of 54 ± 4 nm), (C) seed particles, (D) nanorice particles with thin shells (13.1 ± 1.1 nm), and (E) nanorice particles with thick shells (27.5 ± 1.7 nm).

also see that the plasmon tunability arising from varying the thickness of the shell layer is far more geometrically sensitive than that arising from varying the length of the nanostructure.

The fabrication of nanorice involves seeded metallization of spindle-shaped hematite nanoparticle cores (see the Supporting Information) (Figure 1A). Small Au nanoparticles (~2 nm in diameter) are immobilized onto the surface of (3-aminopropyl) trimethoxysilane (APTMS) functionalized cores at a nominal coverage of ~30%. The immobilized Au colloids act as nucleation sites for electroless Au plating onto the surface of core particles, leading to the gradual formation of a continuous and complete Au shell layer. This is essentially the same metallization procedure used in silica−Au nanoshell synthesis[12] and shows that this approach is readily adaptable to produce uniform metallization layers on the surfaces of other oxide nanoparticles. Further metal deposition onto the nanostructure increases the thickness of the metal layer. Nanorice can be dispersed homogeneously in solvents such as water and ethanol to form colloidal solutions or be dispersed and immobilized on polyvinylpyridine (PVP)-coated substrates as individual, randomly oriented nanoparticles.

Extinction spectra of nanorice with varying thicknesses of the shell layer are shown in Figure 2A (a representative SEM image of the nanorice sample used to obtain these optical measurements is shown in Figure 2B). The strong plasmon resonance feature observed in the spectra in Figure 2A arises because of the longitudinal plasmon of this layered structure and exhibits a highly sensitive structural dependence of its optical resonance, which blueshifts as the metal layer thickness is increased. A finite difference time domain (FDTD) analysis[22] of the far field extinction spectrum of this nanostructure reveals that the transverse plasmon mode (Figure 2C inset) has a much weaker extinction cross section than the longitudinal mode of this nanostructure (Figure 2C). The weaker, higher energy resonance observed in the spectrum of nanorice is attributable to the far weaker transverse plasmon mode, with a small additional contribution from a higher order longitudinal plasmon mode. The local fields associated with the longitudinal and transverse nanorice plasmons are shown in Figure 2D and E. Here we see that the asperities of this structure support very strong local field intensity enhancements (>7000 for this specific nanorice geometry) at wavelengths corresponding to the

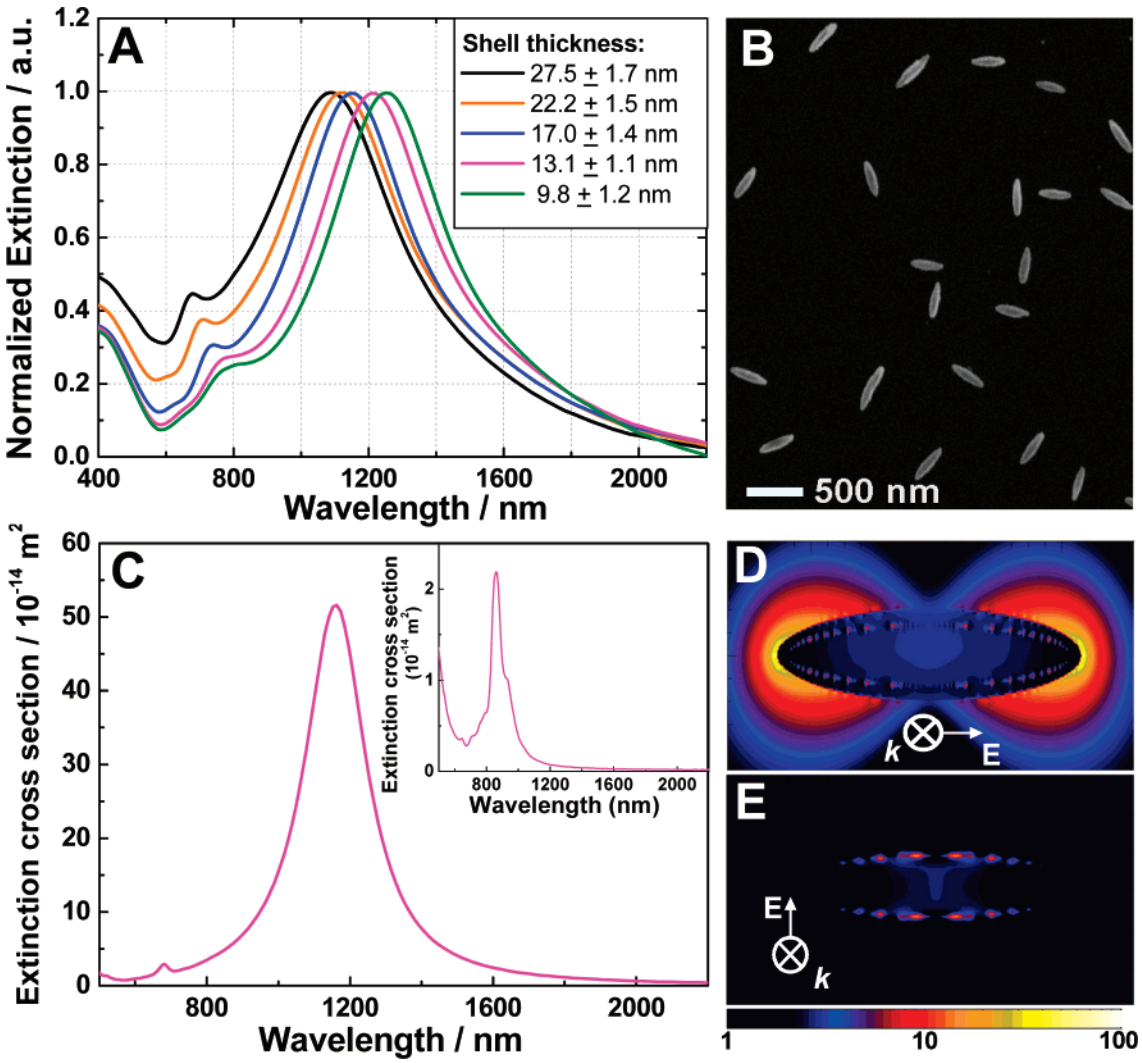

Figure 2. (A) Extinction spectra of hematite−Au core−shell nanorice with different shell thicknesses. Two plasmon peaks are observed for each sample. The plasmons at longer and shorter wavelengths are the longitudinal and transverse plasmons, respectively. The samples measured are monolayers of isolated nanoshells immobilized on PVP-glass slides. (B) A SEM image of a monolayer of nanorice particles (shell thickess of 13.1 ± 1.1 nm) on a PVP-glass slide. (C) Calculated far-field extinction spectra of the nanorice with incident polarization along the longitudinal and (inset) transverse axis of a nanorice particle using FDTD. The nanorice particle employed for the FDTD simulations is composed of a hematite core with longitudinal diameter of 340 nm and transverse diameter of 54 nm surrounded by a 13-nm-thick Au shell. Near-field profile of the nanorice under resonance excitations: (D) incident polarization along the longitudinal axis, $\lambda_{ex} = 1160$ nm; (E) incident polarization along the transverse axis, $\lambda_{ex} = 860$ nm.

longitudinal plasmon resonance of the nanostructure. This intensity enhancement is several times larger than those reported for nanofabricated bowtie junctions[23] and what has been predicted and measured in scanning probe junctions.[24,25] Such strong, tunable local fields make this geometry highly attractive for use in designing substrates for surface-enhanced spectroscopy-based sensing. These large plasmon resonant local field enhancements are similar in magnitude to the localized plasmon resonant "hot spots" occurring in junctions between metallic nanoparticles when a dimer plasmon resonance is excited.[26−28] The nanorice local fields should give rise to intense SERS enhancements with the added advantage that the hot spots are completely open to the surrounding medium in this geometry. From this point of view, each nanorice particle can potentially serve as a standalone, optically addressible nanoscale substrate for surface-enhanced spectroscopies. Moreover, because the enhanced near-field intensities can extend several tens of nanometers from the surface of the nanorice, these particles may exhibit unique advantages in the spectroscopic sensing and characterization of large biomolecules, such as proteins and DNA, biological samples, or materials placed directly adjacent to the nanoparticle.

Nanorice plasmons can be understood by applying the plasmon hybridization picture to this geometry (Figure 3). The sphere-cavity model for spherical nanoshells[20,21] can be generalized to describe the plasmon resonances of nanorice, as the hybridization between plasmon modes of a solid prolate spheroid and an ellipsoidal cavity inside a continuous metal (see the Supporting Information).

For a solid prolate spheroidal particle of aspect ratio (semimajor/semiminor axis) = coth α consisting of a metal with an electron density corresponding to a bulk plasmon frequency ω_B, a metallic background polarizability of ϵ_S,

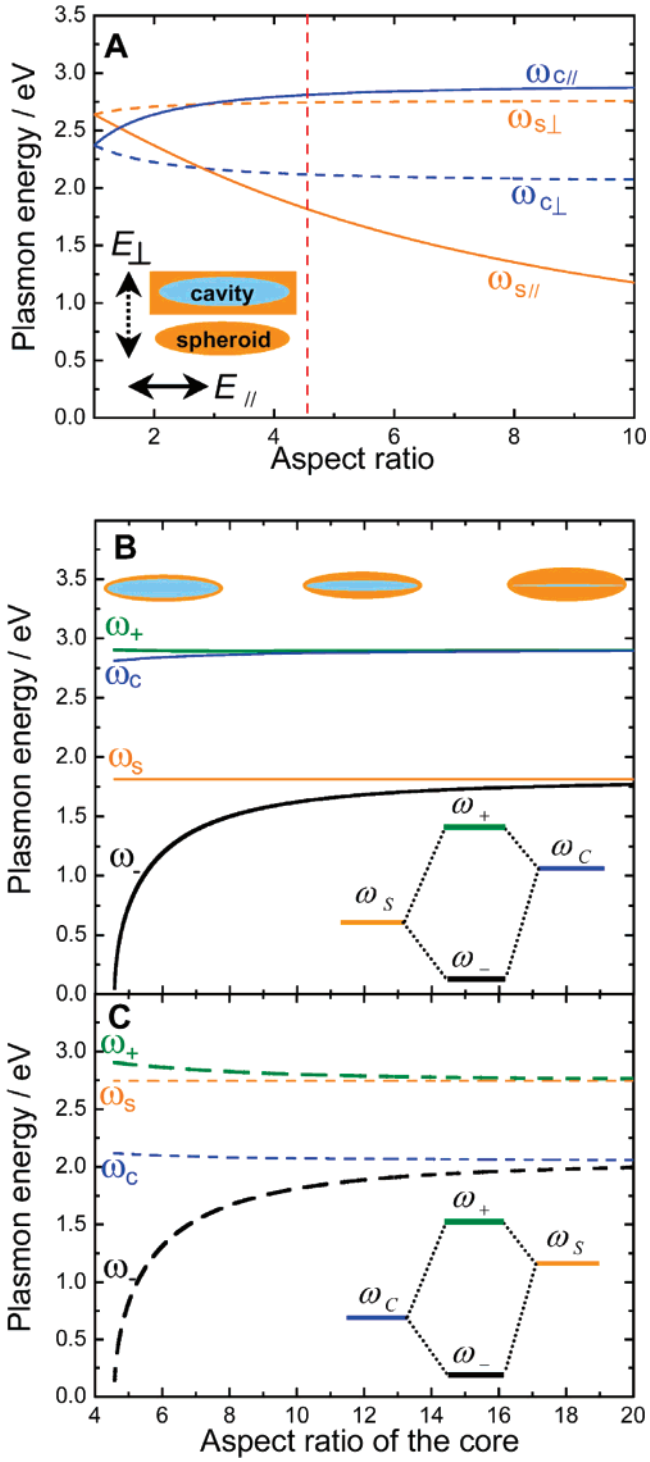

Figure 3. Simulation of the plasmonic properties of nanorice using the plasmon hybridization model: (A) Plasmon energy vs aspect ratio (major radius/minor radius) of the solid prolate spheroid and prolate cavity. The solid lines refer to longitudinal polarization, and the dashed lines refer to transverse polarization. Plots of (B) longitudinal and (C) transverse plasmon energies vs core aspect ratio of a nanorice particle. The aspect ratio of the spheroid is fixed at 4.575. The orange and blue lines indicate the relevant plasmon energies of the solid prolate spheroid and the prolate cavity modes, respectively. The black and green lines refer to bonding (w_-) and antibonding (w_+) plasmons, respectively. The nanorice particle is made up of a metal with a bulk plasmon frequency of 8.95 eV and a core dielectric of 9.5.

immersed in a dielectric with permittivity ϵ_E, the energies of the plasmon modes take the following form:

$$\omega^2_{S,lm}(\alpha) = \omega^2_B \frac{P'_{lm}(\cosh\alpha)Q_{lm}(\cosh\alpha)}{\epsilon_S P'_{lm}(\cosh\alpha)Q_{lm}(\cosh\alpha) - \epsilon_E P_{lm}(\cosh\alpha)Q'_{lm}(\cosh\alpha)} \quad (1)$$

For a prolate dielectric cavity of aspect ratio coth α filled with a dielectric medium of permittivity ϵ_C in the same metallic material, the plasmon energies are

$$\omega^2_{C,lm}(\alpha) = \omega^2_B \frac{P_{lm}(\cosh\alpha)Q'_{lm}(\cosh\alpha)}{\epsilon_S P_{lm}(\cosh\alpha)Q'_{lm}(\cosh\alpha) - \epsilon_C P'_{lm}(\cosh\alpha)Q_{lm}(\cosh\alpha)} \quad (2)$$

In Figure 3A, we show the dependence on aspect ratio of the transverse and longitudinal plasmon resonances of an Au nanorod, modeled as a prolate spheroid (eq 1) and that of an elliptical dielectric cavity embedded in an infinite Au volume (eq 2). Each of these nanostructures supports longitudinal and transverse plasmon resonances dependent strongly upon aspect ratio, where an aspect ratio of 1 corresponds to the spherical particle and cavity case. The cavity plasmon described here corresponds to a void filled with a dielectric medium of dielectric constant $\epsilon_C = 9.5$, that of hematite. For this large dielectric function the cavity is strongly redshifted to energies lower than the solid spheroid plasmon resonance. As the aspect ratio increases, the energies of the longitudinal plasmon of the spheroid and the transverse plasmon of the cavity decrease, while the longitudinal plasmon of the cavity and the transverse plasmon of the spheroid increase. Varying the aspect ratio of the cavity and spheroid shifts the relative energy of the cavity and spheroid parent plasmon modes, which ultimately affects the way in which the cavity and spheroid plasmon states hybridize in the nanorice geometry.

The nanorice plasmon resonances are determined by a hybridization of the parent spheroid and cavity plasmon resonances corresponding to the aspect ratio of the nanoparticle. The outer aspect ratio chosen is 4.575, corresponding to the 366 nm × 80 nm dimensions of the experimentally realized nanorice and denoted by the dashed red line in Figure 3A. For this aspect ratio, we show how the nanorice resonances vary as the aspect ratio of the core is varied while the overall particle size and aspect ratio of the nanoparticle are held constant, for the longitudinal (Figure 3B) and transverse (Figure 3C) resonances of the nanostructure. As the aspect ratio of the core is decreased, the hybridization between the cavity and spheroid modes becomes progressively stronger, resulting in larger energy gaps between the bonding and antibonding plasmon modes. The lower energy "bonding" plasmon modes of nanorice are much more sensitive to the core and shell dimensions than the "antibonding" plasmon modes for both the longitudinal and the

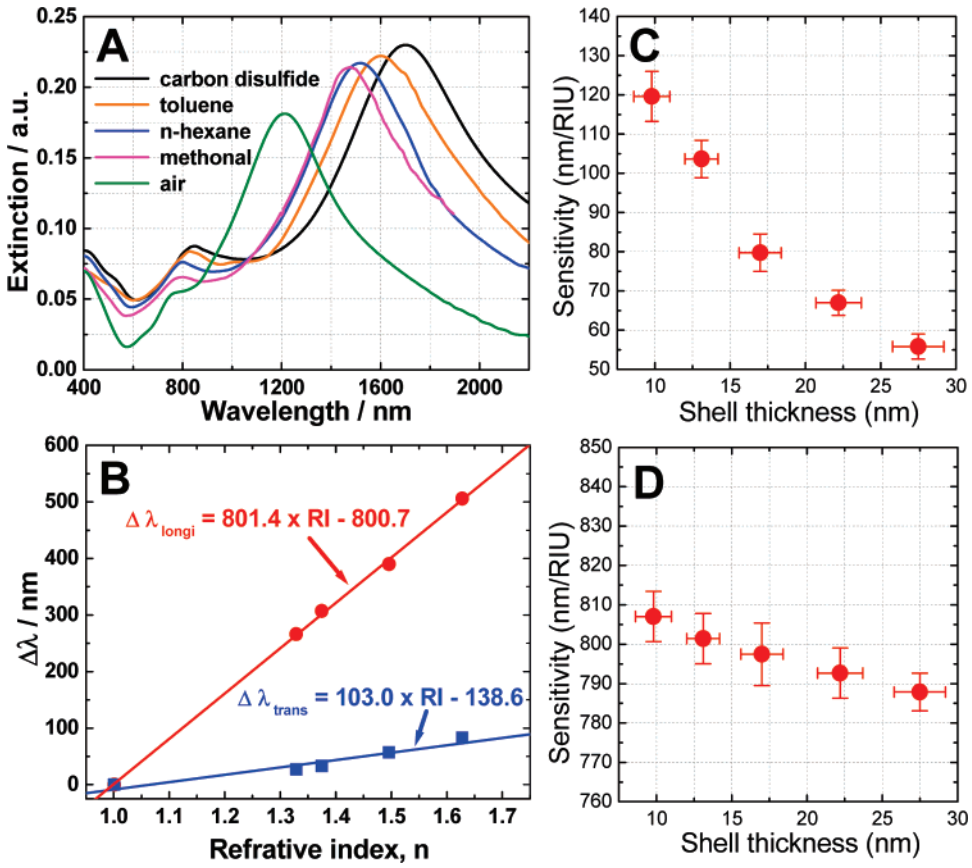

Figure 4. SPR sensing using nanorice: (A) Extinction spectra of a monolayer film of nanorice (shell thickess of 13.1 ± 1.1 nm) immersed in different solvents. (B) The shift of the longitudinal and transverse plasmon energies as a function of the solvent refractive index. The SPR sensitivity based on the longitudinal and transverse plasmons is 801.4 and 103.0 nm/RIU, respectively. The sensitivity of the (C) transverse and (D) longitudinal plasmons of nanorice as a function of the shell thickness. The SPR sensitivity decreases as the shell thickness increases. The SPR sensitivity of the transverse plasmon is more dependent on shell thickness than that of the longitudinal plasmon.

transverse case. The nanorice plasmon modes have a significantly increased geometric sensitivity and can be tuned across a broader spectral range than the parent solid spheroid and cavity plasmon modes. In particular, the low-energy "bonding" plasmon extends toward zero frequency in the thin shell limit, for both the transverse and longitudinal case. For longitudinal polarization, the nature of the bonding plasmon is solid-particle-like and the antibonding mode is cavity-like. For transverse polarization, the situation is reversed. Because the energy of the cavity plasmon for transverse polarization is lower than the energy of the solid spheroid plasmon, the nature of the bonding plasmon is cavity-like and the antibonding mode is solid-particle-like. Because the solid spheroidal plasmons have a much larger induced dipole moment and couple more strongly to incident light than cavity-like plasmons, the extinction cross section for longitudinal polarization is dominated by the bonding nanorice plasmon and for transverse polarization, the spectrum is dominated by the antibonding plasmon mode, which was indeed observed (Figure 2).

The longitudinal nanorice plasmon resonance wavelength is highly sensitively dependent on surrounding dielectric media, with a sensitivity as high as 801 nm RIU^{-1} (RIU = refractive index unit). To the best of our knowledge, the longitudinal plasmon of nanorice exhibits the largest SPR sensitivity among all of the experimentally realizable metal nanostructures reported thus far, including triangular nanoprisms,[29] nanorods,[18] spherical nanoshells,[30,31] and nanocubes.[32] This was studied by exposing a monolayer of isolated nanorice particles immobilized on a PVP-coated glass slide to solvents with varying refractive indices. Both the longitudinal and transverse plasmons of nanorice redshift as the refractive index of solvents increases with a linear dependence of plasmon wavelength on the refractive index, as is characteristic of other nanoparticle structures.[18,29−32] The longitudinal plasmon is far more sensitive to the change of the dielectric medium than the transverse plasmon, at 103 nm RIU^{-1}. The difference in SPR sensitivity between the longitudinal and transverse nanorice plasmons can also be explained in the context of the plasmon hybridization model, where the spheroid-like plasmon resonance has increased sensitivity to changes in its dielectric environment while a cavity-like resonance has greater sensitivity to changes in the dielectric properties within the nanoparticle core.[21] The experimentally measured SPR shifts of the longitudinal and transverse plasmons are in very good agreement with theory, according to both FDTD simulations (1060 nm RIU^{-1} and 115 nm RIU^{-1}) and plasmon hybridization modeling (620 nm RIU^{-1} and 80 nm RIU^{-}). Figures 4C and D show the SPR sensitivity of nanorice plasmons as a function of Au shell thickness. The SPR sensitivity of the longitudinal plasmon is maintained as shell thickness is varied, whereas

that of the transverse plasmon decreases as shell thickness increases. Such environmental sensitivity of the plasmons of nanorice holds great potential for monitoring local environmental changes during chemical and biological processes.

In summary, nanorice is an important new geometry for plasmonic nanoparticles, combining the highly attractive nanoscale optical properties of both nanorods and nanoshells. The unique properties of this new nanostructure are highly attractive for applications such as standalone nanosensors exploiting surface-enhanced spectroscopies or SPR sensing modalities. Applying the plasmon hybridization model as design principles to realizable nanostructures will result in the selective implementation of optimized optical properties into structures and devices of mesoscale dimensions.

Acknowledgment. This work is supported by the National Science Foundation (NSF) Grant EEC-0304097, Air Force Office of Scientific Research Grant F49620-03-C-0068, National Aeronautics and Space Administration (NASA) Grant 68371, Robert A Welch Foundation Grants C-1220 and C-1222, Multidisciplinary University Research Inititative (MURI) W911NF-04-01-0203, and the NSF-funded Integrative Graduate Research and Educational Training (IGERT) program in Nanophotonics.

Supporting Information Available: Experimental details and details of the plasmon hybridization model applied to the nanorice system. This material is available free of charge via the Internet at http://pubs.acs.org.

References

(1) Raether, H. *Surface Plasmon on Smooth and Rough Surfaces and on Gratings*; Springer: Berlin, Germany, 1988.
(2) Kreibig, U.; Vollmer, M. *Optical Properties of Metal Clusters*; Springer-Verlag: Berlin, Germany, 1995.
(3) Maier, S. A.; Brongersma, M. L.; Kik, P. G.; Meltzer, S.; Requicha, A. A. G.; Atwater, H. A. *Adv. Mater.* **2001**, *13*, 1501.
(4) Xia, Y.; Halas, N. *MRS Bull.* **2005**, *30*, 338.
(5) Barnes, W. L.; Dereux, A.; Ebbesen, T. W. *Nature* **2003**, *424*, 824.
(6) Maier, S. A.; Atwater, H. A. *J. Appl. Phys.* **2005**, *98*, 011101.
(7) Ozbay, E. *Science* **2006**, *311*, 189.
(8) Link, S.; El-Sayed, M. A. *J. Phys. Chem. B* **1999**, *103*, 8410.
(9) Murphy, C. J.; Sau, T. K.; Gole, A.; Orendorff, C. J. *MRS Bull.* **2005**, *30*, 349.
(10) Aizpurua, J.; Hanarp, P.; Sutherland, D. S.; Kall, M.; Bryant, G. W.; de Abajo, F. J. G. *Phys. Rev. Lett.* **2003**, *90*, 057401.
(11) Sun, Y. G.; Xia, Y. N. *Science* **2002**, *298*, 2176.
(12) Oldenburg, S. J.; Averitt, R. D.; Westcott, S. L.; Halas, N. J. *Chem. Phys. Lett.* **1998**, *288*, 243.
(13) Nie, S.; Emory, S. R. *Science* **1997**, *275*, 1102.
(14) Kneipp, K.; Wang, Y.; Kneipp, H.; Perelman, L. T.; Itzkan, I.; Dasari, R. R.; Feld, M. S. *Phys. Rev. Lett.* **1997**, *78*, 1667.
(15) Xu, H. X.; Bjerneld, E. J.; Kall, M.; Borjesson, L. *Phys. Rev. Lett.* **1999**, *83*, 4357.
(16) Michaels, A. M.; Nirmal, M.; Brus, L. E. *J. Am. Chem. Soc.* **1999**, *121*, 9932.
(17) Jackson, J. B.; Halas, N. J. *Proc. Natl. Acad. Sci. U.S.A.* **2004**, *101*, 17930.
(18) Link, S.; Mohamed, M. B.; El-Sayed, M. A. *J. Phys. Chem. B* **1999**, *103*, 3073.
(19) Murphy, C. J.; Jana, N. R. *Adv. Mater.* **2002**, *14*, 80.
(20) Prodan, E.; Radloff, C.; Halas, N. J.; Nordlander, P. *Science* **2003**, *302*, 419.
(21) Prodan, E.; Nordlander, P. *J. Chem. Phys.* **2004**, *120*, 5444.
(22) Oubre, C.; Nordlander, P. *J. Phys. Chem. B* **2004**, *108*, 17740.
(23) Schuck, P. J.; Fromm, D. P.; Sundaramurthy, A.; Kino, G. S.; Moerner, W. E. *Phys. Rev. Lett.* **2005**, *94*, 017402.
(24) Sanchez, E. J.; Novotny, L.; Xie, X. S. *Phys. Rev. Lett.* **1999**, *82*, 4014.
(25) Hartschuh, A.; Sanchez, E. J.; Xie, S. X.; Novotny, L. *Phys. Rev. Lett.* **2003**, *90*, 095503.
(26) Michaels, A. M.; Jiang, J.; Brus, L. *J. Phys. Chem. B.* **2000**, *104*, 11965.
(27) Nordlander, P.; Oubre, C.; Prodan, E.; Li, K.; Stockman, M. I. *Nano Lett.* **2004**, *4*, 899.
(28) Gunnarsson, L.; Rindzevicius, T.; Prikulis, J.; Kasemo, B.; Kall, M.; Zou, S. L.; Schatz, G. C. *J. Phys. Chem. B* **2005**, *109*, 1079.
(29) Haes, A. J.; Van Duyne, R. P. *J. Am. Chem. Soc.* **2002**, *124*, 10596.
(30) Sun, Y. G.; Xia, Y. N. *Anal. Chem.* **2002**, *74*, 5297.
(31) Tam, F.; Moran, C. E.; Halas, N. J. *J. Phys. Chem. B.* **2004**, *108*, 17290.
(32) Sherry, L. J.; Chang, S.-H.; Schatz, G. C.; Van Duyne, R. P.; Wiley, B. J.; Xia, Y. N. *Nano Lett.* **2005**, *5*, 2034.

NL060209W

Nanorice: a Hybrid Plasmonic Nanostructure

Hui Wang,[1,4] Daniel W. Brandl,[2,4] Fei Le,[2,4] Peter Nordlander,[2,3,4] Naomi J. Halas*[,1,3,4]

[1] *Department of Chemistry,* [2] *Department of Physics and Astronomy,* [3] *Department of Electrical and Computer Engineering, and* [4] *the Laboratory for Nanophotonics, Rice University, Houston, TX, 77005*

* To whom correspondence should be addressed. Email: halas@rice.edu

Experimental details:

Ferric chloride ($FeCl_3$•$6H_2O$), (3-aminopropyl)trimethoxysilane (APTMS, 97%), tetrachloroauric acid ($HAuCl_4$•$3H_2O$), tetrakis hydroxymethyl phosphonium chloride (THPC) were purchased from Sigma-Aldrich (St. Louis, MO). 37% formaldehyde, potassium dihydrogen phosphate (KH_2PO_4) and 200-proof ethanol were obtained from Fisher Scientific (Hampton, NH). All the chemicals were used as received without further purification. Ultrapure water (18.2 MΩ resistivity) was obtained from a Milli-Q water purification system (Millipore, Billerica, MA).

Monodisperse spindle-shaped hematite particles with controllable aspect ratios were fabricated by forced hydrolysis of ferric chloride solutions.[1] Hematite particles with aspect ratio of 6.3 (340 nm x 54 nm) were prepared by aging 100 mL of aqueous solution containing 2.0 x 10^{-2} M $FeCl_3$ and 4.0 x 10^{-4} M KH_2PO_4 at 100 ^{o}C for 72 hours. The resulting precipitate was centrifuged and washed several times with water and ethanol. Finally, the precipitate was redispersed in 25 mL ethanol.

The seed particles used in the present study were fabricated following a similar procedure as the previously reported method for the immobilization of Au nanoparticles on silica surfaces. The surface of the spindle-shaped hematite particles was functionalized with organosilane molecules (APTMS) to generate an amine moiety coated surface. Typically, 600 μL of APTMS was introduced into 5 mL of ethanolic solution of hematite particles under vigorous stir. The surface functionalization of hematite particles were accomplished by stirring the mixture for 12 hours. The resulting particles were centrifuged and redispersed in ethanol several times to get rid of the excess APTMS. THPC-capped Au nanoparticles (~2 nm in diameter) were prepared following Duff's method,[2] and then attached to the functionalized hematite particle surfaces through the gold-amine interactions.[3] These attached Au colloids acted as the nucleation sites for the reduction of Au ions from solution onto the hematite surface until continuous and complete Au nanoshells were formed.[4]

Nanorice particles were fabricated via seed-catalyzed reduction of $AuCl_4^-$ ions by formaldehyde in

aqueous solutions at room temperature. The growth of complete Au shells typically took 5-10 min. By adjusting the amount ratio between seed particles and $AuCl_4^-$ ions, the thickness of the Au shells can be precisely controlled. The resulting nanorice particles can be homogenously dispersed in water to form colloidal solutions.

Nanorice films were prepared by immobilizing nanorice particles on polyvinylpyridine (PVP)-coated glass substrates.[5,6] Briefly, glass slides were cleaned in piranha solution (sulfuric acid : hydrogen peroxide, 7:3) and immersed in a 1% wt. solution of PVP in ethanol for 24 hours. The slides were rinsed thoroughly with ethanol and dried with N_2 gas. The PVP-functionalized slides were immersed in an aqueous solution of nanorice for 1 hour. Upon removal from the nanorice solution, the films were rinsed with ethanol and dried with N_2. This resulted in a monolayer of isolated nanorice particles with random orientations.

Scanning electron microscope (SEM) images were obtained on a Phillips FEI XL-30 environmental scanning electron microscope at an acceleration voltage of 30 kV. The samples for SEM measurements were prepared by drying a drop of colloidal solutions on silicon wafer surface under ambient air. TEM images were obtained using JEOL JEM-2010 transmission electron microscope. The extinction spectra were obtained using a Cary 5000 UV/Vis/NIR spectrophotometer in the wavelength range of 400 nm to 2400 nm.

Plasmon hybridization:

The plasmon hybridization method can be used to describe the plasmon modes of the nanorice particles in a manner analogous to the plasmon modes in the spherical nanoshell system.[7] The plasmons can be viewed as resulting from hybridization of the aspect-ratio-dependent primitive plasmon modes of a solid metallic prolate spheroid and the primitive plasmon modes of a prolate spheroidal dielectric cavity in a uniform metallic background. For simplicity we assume a uniform metallic electron density of n_0 corresponding to a bulk plasmon energy $\omega_B = \sqrt{\frac{4\pi n_0 e^2}{m_e}}$.

The scalar potential used in the plasmon hybridization method to describe the deformations of the electron liquid in a prolate spheroidal system takes the form: [8]

$$\eta = \sum_{lm} [\dot{S}_{lm}(t) P_{lm}(\cosh\alpha) + \dot{C}_{lm}(t) Q_{lm}(\cosh\alpha)] P_{lm}(\cos\beta) e^{im\phi} ,$$

where S_{lm} are the amplitudes for the primitive plasmons of the solid particle, and C_{lm} are the amplitudes for the primitive plasmons of a cavity. The functions P_{lm} and Q_{lm} are the associated Legendre

polynomials of the first and second kind. In prolate spheroidal coordinates, the surface of constant α is an elliptical spheroid, and cothα is the aspect ratio of the spheroid that is formed.[8]

Prolate spheroidal coordinates are defined with a unique focal length, and the nanorice particles are modeled by confocal ellipsoidal shells. The outer and inner surface of the shell will therefore have different aspect ratios and the shell thickness will be nonuniform. The Lagrangian for the nanorice particles is diagonal in multipolar indices *lm*. For this reason, the nanorice plasmons can be expressed as bonding and antibonding modes resulting from an interaction between a solid particle plasmon and a cavity plasmon of a common multipolar index *lm*.

A straightforward application of the plasmon hybridization method to a solid prolate spheroid of aspect ratio cothα gives the following plasmon modes:

$$\omega_{S,lm}^2(\alpha) = \omega_B^2 \frac{P'_{lm}(\cosh\alpha)Q_{lm}(\cosh\alpha)}{\varepsilon_S P'_{lm}(\cosh\alpha)Q_{lm}(\cosh\alpha) - \varepsilon_E P_{lm}(\cosh\alpha)Q'_{lm}(\cosh\alpha)},$$

where ε_S is the background polarizability of the metal and ε_E is the dielectric permittivity of a possible embedding medium. The plasmon energies of a prolate spheroidal cavity filled with a medium with dielectric permittivity ε_C take the form:

$$\omega_{C,lm}^2(\alpha) = \omega_B^2 \frac{P_{lm}(\cosh\alpha)Q'_{lm}(\cosh\alpha)}{\varepsilon_S P_{lm}(\cosh\alpha)Q'_{lm}(\cosh\alpha) - \varepsilon_C P'_{lm}(\cosh\alpha)Q_{lm}(\cosh\alpha)}.$$

The presence of dielectrics plays a large role in the plasmon frequencies of the solid spheroid and cavity. For the nanorice particles, which contain a hematite core with a dielectric constant of approximately $\varepsilon_C = 9.5$, the cavity mode lies below the spheroid mode for the transverse polarization for all aspect ratios. For the aspect ratio considered in the present paper, $\varepsilon = 4.575$, the cavity plasmon lies above the solid spheroid mode for longitudinal polarization.

The nature of the plasmon modes in a shell particle depends on the relative position of the primitive plasmons. For transverse polarization, the bonding nanorice plasmon is primarily composed of the cavity plasmon while the antibonding mode is solid particle-like. In a shell geometry, the multipolar moments of the cavity plasmons are smaller than those of the solid particle plasmons. In the electrostatic limit, the probability for excitation of a plasmon mode is proportional to the square of its dipole moment.[7] For this reason, for longitudinal polarization, the bonding plasmon is much brighter than the antibonding plasmon. For the transverse modes, the situation is reversed and the antibonding plasmon is much brighter than the bonding plasmon.

Reference:

(1) Ozaki, M.; Kratohvil, S.; Matijevic, E. *J. Colloid Interface Sci.* **1984**, *102*, 146-151.
(2) Duff, D. G.; Baiker, A.; Edwards, P. P. *Langmuir* **1993**, *9*, 2301-2309.
(3) Westcott, S. L.; Oldenburg, S. J.; Lee, T. R.; Halas, N. J. *Langmuir* **1998**, *14*, 5396-5401.
(4) Oldenburg, S. J.; Averitt, R. D.; Westcott, S. L.; Halas, N. J. *Chem Phys Lett* **1998**, *288*, 243-247.
(5) Malynych, S.; Luzinov, I.; Chumanov, G. *J Phys Chem B* **2002**, *106*, 1280-1285.
(6) Tam, F.; Moran, C. E.; Halas, N. J. *J. Phys. Chem. B.* **2004**, *108*, 17290-17294.
(7) Prodan, E.; Nordlander, P. *J. Chem. Phys.* **2004**, *120*, 5444-5454.
(8) Vinogradov, S. S.; Smith, P. D.; Vinogradova, E. D. *Canonical problems in scattering and potential theory*; Chapman & Hall/CRC: Boca Raton, Florida, 2001.